This document is the unedited Author's version of a Submitted Work that was subsequently accepted for publication in ACS Applied Materials & Interfaces, copyright © American Chemical Society after peer review. To access the final edited and published work see: 10.1021/acsami.2c10656

Leveraging solidification dynamics to design robust ice-shedding surfaces

*Michael J. Wood, Gregory Brock, Phillip Servio, Anne-Marie Kietzig**

McGill University Department of Chemical Engineering, Montréal, Canada, H3A 0C5

*Corresponding author: anne.kietzig@mcgill.ca

KEYWORDS

Anti-icing, Ice-shedding, Ice-adhesion, Solidification, Stress-concentration

ABSTRACT

The adhesion of ice to external surfaces is an important challenge in many industries. This has sparked much research into fabricating surfaces with low ice adhesion strengths. Our novel approach to designing ice-shedding surfaces leverages the dynamics of water solidification to induce beneficial stress concentrations throughout the iced interface. We have chosen a bare woven metal wire cloth substrate to demonstrate these principles. The pore geometries of the wire cloths lead to stress concentrations upon freezing and expansion of the water/ice, while their microstructural topography allows for facile crack opening. We have discovered that by leveraging knowledge of the underlying physical processes involved in ice formation and delamination, we can engineer a robust metal surface to have extremely low ice adhesion strength (12.5 kPa) without using chemical coatings.

INTRODUCTION

The adhesion of ice to external surfaces has been a persistent engineering challenge which ranges from a mere nuisance to a severe safety concern [1]. This includes the adhesion of ice to metallic structures such as the wings and fuselages of aircraft [2]. There has, therefore, been much research published on surfaces which more easily shed bound ice. The typical benchmark used to classify surfaces as “pagophobic” (icephobic) is an ice adhesion strength $\tau_{ice} < 100$ kPa [3, 4]. However, some have noted that passive removal of ice will only occur when $\tau_{ice} < 20$ kPa [5] while others set the benchmark even lower at $\tau_{ice} < 0.1$ kPa [6]. For context, flat, rigid metals typically present with ice adhesion strengths on the order of 1000 kPa [7].

To date there have broadly been two prevailing paradigms for the engineering of low ice adhesion strength surfaces, both of which attempt to tune the work of adhesion. The first method is to apply a low surface energy coating or an infused sacrificial lubricating film to the surface [5, 8-11]. While these additional coatings on top of the substrate material have yielded exceptionally low ice adhesion strengths, in many cases they have been shown to lack robustness even in laboratory testing [12, 13]. The second prevailing research paradigm has been to leverage knowledge of superhydrophobic surface engineering, where favourable topographies are employed to trap air between asperities – limiting water-solid (and, in theory, ice-solid) contact area [10, 14-19]. These results have been overall mixed; there is a growing consensus that hydrophobicity does not naturally lead to pagophobicity. The first consideration is that wettability is typically measured on a goniometer using water droplets of approximately 5 μl compared to the much smaller $5\text{x}10^{-6}$ μl droplets typically found in clouds [20]. The second consideration is that as temperatures are decreased past the dew point, water molecules from humid air will adsorb onto cold surfaces, regardless of intrinsic wettability [21]. This adsorption of water effectively renders the surface hydrophilic and the air trapping effect of superhydrophobic surfaces is lost, with water infiltrating the asperities before solidification to ice occurs. The result is often higher ice adhesion strengths measured on superhydrophobic surfaces than smooth surfaces of the same material due to increased ice-substrate interlocking [1, 14, 19].

While the tuning of the work of adhesion has been broadly studied, what has been largely lacking in pagophobic surface engineering research is a consideration of the actual mechanics of the ice-substrate bond failure. Practically speaking, for solid ice to be delaminated from a substrate when a force is applied, (i) cracks must initiate; and (ii) these cracks must advance across the length of the iced area. The aim for an ice-shedding surface is that crack initiation and advancement occurs with minimal energy, and exclusively at the ice-solid interface – leading to adhesional failure. The importance of crack initiation/advancement consideration is demonstrated by the work of Golovin et al. (2019) who tested the force required to dislodge ice of varying bonded lengths. It was shown that dislodging force does not scale continuously with bonded area, but rather an asymptotic force is reached at a critical bonded length. The shear strength of the ice-solid interface controls delamination when the length of the interface is relatively small; propagation of the interfacial crack controls delamination when the length of the interface is relatively large [22]. Recently, Al-rich quasicrystalline alloys have been shown to have a low interfacial toughness with bonded ice, leading to shear strengths of approximately 30 kPa when the bonded length is 20 cm [23].

There have been a few recent studies which try to directly manipulate ice crack initiation and propagation on elastomers. Golovin et al. (2016) altered the crosslink density of polydimethylsiloxane (PDMS) samples, with the goal of increasing material compliance and inducing cavitation at the ice-solid interface [24]. However, low values of shear modulus lead to low mechanical durability. Irajizad et al. (2019) attempted to overcome these limitations by creating a silicone elastomer material consisting of a low-modulus phase within a high-modulus matrix. As force is applied to adhered ice, stress is localized at the regions containing the low-modulus phase, leading to crack initiation and a reduction in ice adhesion strength by a factor of 800 compared to an aluminum control sample [25]. Similarly, Sivakumar et al. (2021) have recently published their work on incorporating a polyurethane elastomer into grooves machined onto the surface of aluminum. The compliant elastomer fraction of the surface aids in ice shedding, while the aluminum fraction increases wear resistance [26]. He et al. have published extensively on the initiation of macro-scale cracks at the interface between ice and their PDMS substrates. These macro-crack initiation sites originate from an inhomogeneity in the stiffness of the substrate and adhered ice [27]. Their engineering of hollow structures within the PDMS results in greater deformation/buckling of the substrate once a shear force is applied to the adhered ice while avoiding any interlocking between the ice and the surface. These hollow sub-surface structures present with ice adhesion strengths about half of what is measured on flat monolithic PDMS [27-30].

There has been recent progress towards fabricating ice crack inducing surfaces out of bare metals. Specifically, Zarasvand et al. (2021) have fabricated ice-shedding surfaces from thin metal sheets which are suspended using narrow strips of double-sided tape to allow them to deform in a manner similar to elastomeric systems [31]. And previous work from our laboratory by Ling et al. (2016) showed that woven wire cloths present with exceptionally low ice adhesion strengths [14].

In this work, we intend to show that a robust ice-shedding surface can be made exclusively of bare metal by leveraging knowledge of water solidification dynamics to induce cracks at the ice-substrate interface. That is, favourable surface structures can be engineered to both form stress concentration sites throughout the iced interface, and to offer an energetically favourable path for cracks to follow to completely delaminate the bonded ice.

EXPERIMENTAL PROCEDURE

Metal Substrate Preparation

Ultra-fine 316 stainless-steel Dutch twill weave wire cloths, typically used as filtration media, served as the substrate in this study (Dorstener Wire Tech., Inc., Spring, TX, United States). As shown in the rendering of Figure 1, these cloths are composed of warp wires running the width of the material and perpendicular weft wires woven above and below every second warp wire. Differing diameter of wires results in a differing number of warp and weft wires per unit area – the mesh number. In the present work, we tested cloths of three different imperial mesh numbers: 200x1400, 325x2300, and 400x2800. Additionally, 0.036"-thick 316 stainless-steel sheets with a mirror-like #8 finish were purchased to serve as the control surface in the experiments (McMaster-Carr Supply Co., Elmhurst, Il, United States). All substrates were cleaned in a 4-step process before ice adhesion experiments took place. First, the materials were ultrasonically cleaned in acetone for 5 minutes to remove foreign particles. Second, the materials were ultrasonically cleaned in a lactic acid-based detergent, *CLR* (Jelmar, LLC., Skokie, Il, United States) for 45 minutes to remove any weaving or polishing oils. The metal was then generously rinsed with reverse-osmosis water. Finally, the materials were ultrasonically cleaned once more in acetone for 5 minutes to ensure full removal of the detergent.

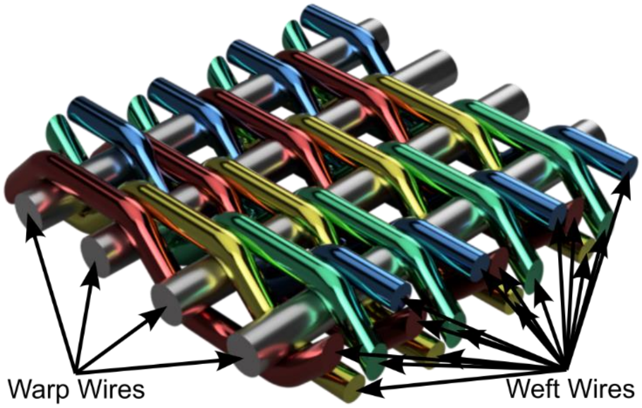

Figure 1. Rendering of the woven wire cloth substrates tested in this work for their ice-shedding properties. Warp wires run the width of the cloth while perpendicular weft wires run the length, weaving above and below every second warp wire.

Polymer Replica Preparation

To obtain a negative template, we cast *Sylgard* 184 polydimethylsiloxane (PDMS, Dow Chemical Co., Midland, MI, United States) in the standard 10:1 weight ratio of monomer to crosslinker over our wire cloth samples and degassed this assembly in a vacuum chamber for 1 hour to remove air bubbles. Next, we cured the PDMS in a 60 ºC oven overnight, then peeled off the PDMS, rinsed it with ethanol and dried it at room temperature before use.

Positive polymer replicas were in turn cast by filling this PDMS mold with polypropylene co-polymer (Total Petrochemicals & Refining, Inc., Houston, TX, United States) which was cryomilled into a powder. The filled mold was placed in a 200 ºC vacuum oven for two hours. The mold was removed from the oven, allowed to cool, and peeled from the polymer replica. A flat, smooth coupon of the same polypropylene material was obtained by injection molding to serve as a control sample. The polypropylene substrates were ultrasonically cleaned in ethanol for 5 minutes before any ice adhesion experiments took place.

Fs-Laser Hole Percussion Drilling

A coupon of the 0.036”-thick stainless-steel sheet was machined with a pattern of through holes via fs-laser micromachining. The cleaned coupon was irradiated using a *Carbide* laser system (Light Conversion, UAB, Vilnius, Lithuania) with a wavelength of 1064 nm, pulse duration of 1 ps, and a repetition rate of 20 kHz. The laser beam was focused onto the surface of the coupon using a 100 mm plano-convex lens. Using a pulse energy of 100 μJ, each though hole was percussion-drilled using 160000 pulses. The percussion-drilled holes were arranged in the same layout as the pores of the 200x1400 wire cloth using XY linear translation stages actuated by a *XPS* universal high-performance motion/driver controller (Newport Corp. Irvine, CA, United States). The machined coupon was cleaned by ultrasonicating in reverse osmosis water for 30 minutes, and stored in reverse osmosis water to maintain hydrophilic surface chemistry.

Sample Characterization

The wire cloth and polymer replica substrates described in the previous sections were imaged using a *Quanta 450* scanning electron microscope (ThermoFisher, Inc., Waltham, MA, United States) both before any ice adhesion experiments took place and after all ice adhesion experiments were completed. An accelerating voltage of 5.0 kV and spot size of 2.5 nm were used to image the stainless-steel samples. Micro-tomography analyses of the three wire cloth substrates were performed using a *Xradia Versa 520* 3D X-ray microscope (Carl Zeiss, AG., Jena, TH, Germany). The collected image slices were reconstructed and segmented using *Dragonfly* (Object Research

Systems, Inc., Montréal, QC, Canada) to visualize the 3D-microstructural networks and extract their total surface areas.

McGill Benchtop Ice Adhesion Testing

The benchtop apparatus used to measure the ice adhesion strengths of the surfaces in this study has been described extensively in previous publications [14, 32]. In brief, the apparatus consists of a *CP-200TT* air-cooled thermoelectric Peltier cooling unit (TE Technology, Inc., Traverse City, MI, United States) which is maintained at a desired cold side temperature setpoint using a proportional-integral control scheme. All the experiments described in the present work were carried out at a setpoint of -15 ºC. The apparatus has been modified since our previous reports to include a custom-built syringe pump, allowing the water to be introduced to the system in a more controlled manner - leading to more consistent results. A schematic of the ice adhesion apparatus is presented in Figure 2.

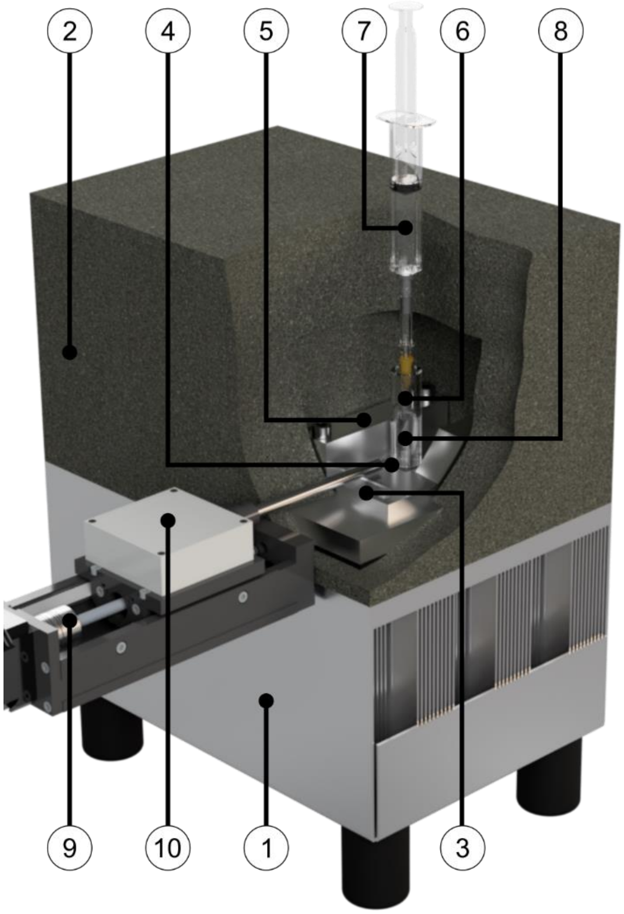

Figure 2. Rendering of the ice adhesion strength testing rig with cutout to show the experimental section. (1) Air-cooled thermoelectric Peltier unit; (2) Insulation of the experimental section; (3) Aluminum base plate; (4) Studied surface; (5) Aluminum sample clamp; (6) Glass tube; (7) Syringe pump; (8) Water/ice column; (9) Motorized linear translation stage; (10) Digital force gauge.

Ice adhesion strength experiments are carried out as follows. First, the studied surface is clamped along two edges to an aluminum base plate sitting on the cold side of the Peltier cooling unit using aluminum bars. A custom-made borosilicate glass tube (Pegasus Industrial Specialties, Inc., Cambridge, ON, Canada) with an outer diameter of 15.9 mm, wall thickness of 2.4 mm, height of

50 mm and fire polished edges is placed onto the studied surface. The thermoelectric cooling unit is then powered on and set to the -15 ºC cold side setpoint; the system is allowed to cool for 30 minutes. Next, a 10 ml syringe equipped with a 23-gauge tip is automatically lowered into the glass tube without touching its wall to dispense, dropwise, 400 µl of chilled reverse osmosis water (-5 - 0 ºC). The syringe is retracted, and the unit is left for 15 minutes. The process is repeated, adding another 400 µl of chilled RO water to the glass tube, creating an ice seal to prevent leakage of water from beneath the tube due to hydrostatic pressure. After an additional 15 minutes, 1700 µl of chilled RO water is added to the glass tube (for a total of 2500 µl) and the experiment is left to freeze undisturbed for 2 hours.

The ice adhesion strengths of the studied substrates were evaluated as the shear stress required to dislodge the ice column from their surfaces. A *ZPS-DPU-22* digital force gauge (Imada, Inc., Northbrook, Il, United States), mounted onto a *T-LSR075B* motorized linear translation stage (Zaber Technologies, Inc., Vancouver, BC, Canada), is driven into the ice column at a rate of 0.5 mm/s. The height of the linear translation stage is adjusted such that the force probe is no more than 1 mm above the specimen to minimize torque. The ice adhesion stress, τ_{ice}, is obtained by dividing the peak force measured when dislodging the ice column by the surface area of the substrate in contact with the ice column. Images were also captured of the tested substrate, underlying aluminum base plate, and ice column interface upon ice dislodging to visualize the contact area of the ice. Ice adhesion tests were repeated 5 – 6 times per substrate (with the exception of the 200x1400 wire cloth which was tested a total of 15 cycles) in the exact same location on their surface, to elucidate any trends with repeated icing cycles.

NRC Altitude Icing Wind Tunnel Experiments

The National Research Council of Canada (NRC) Altitude Icing Wind Tunnel (AIWT) is a closed-loop low-speed wind tunnel oriented in the vertical plane. The AIWT is calibrated according to the SAE ARP 5905 “Calibration and Acceptance of Icing Wind Tunnels". It is used to simulate in-flight atmospheric icing conditions. The full test section has a cross-section of 57×57 cm, where air speeds up to 100 m/s can be reached. For these experiments, a spin rig is installed in the test section which uses cylindrical test probes at the end of 185 mm-long retaining arms attached to a rotating hub (Figure 3 A). The samples are both exposed to the icing cloud and accelerated within the test section, avoiding transfer from one facility to another, and improving experimental repeatability.

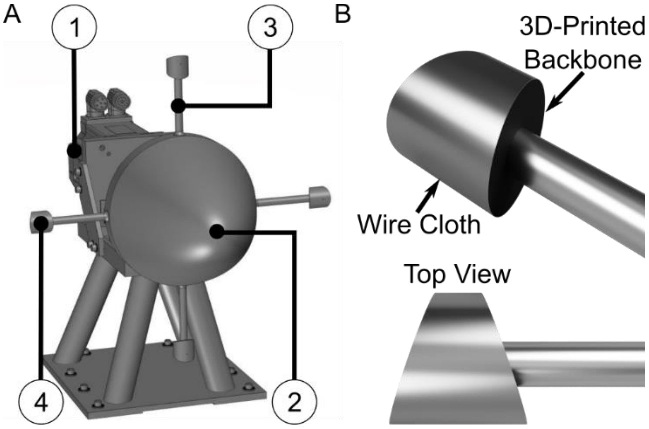

Figure 3. (A) Rendering of the Altitude Icing Wind Tunnel spin rig. (1) Motor; (2) Rotating hub; (3) Retaining arm; (4) Test probe. (B) Rendering of the test probes which consist of a 3D-printed backbone with their faces covered in the wire cloths. The top view illustrates the wedge shape of the test probes which avoids bridging of ice between the arm and the sample.

The cylindrical test probes have a wedge shape which serves to prevent the bridging of ice between the arm and the sample (Figure 3 B). The control test probe was machined from a solid 316 stainless-steel rod (McMaster-Carr) which was then electrochemically polished to a smooth finish. The wire cloth test probes consisted of a 3D-printed backbone with the cloth mounted to its face. The wire cloths were held taut on the surface of the test probes with a bead of epoxy only on the leeward area of the face (i.e. no epoxy was present in the area of the test probe's face where ice accumulated).

The ice adhesion spin rig testing in the NRC AIWT was carried out at the following conditions, simulating a “worst case" in-flight icing condition: static air temperature = -20 ºC, true airspeed at sea level = 80 m/s, median droplet volume diameter = 20 μm, and the liquid water content (LWC) = 0.2 g/m^3. The LWC at the sample locations is verified at the start of the test using a rotating cylinder, which is the standard method used for baseline calibrations at the AIWT. Ice is accreted onto the samples by exposing the slowing-spinning rig (30 RPM) to the super-cooled droplet cloud for 800 s. The droplet cloud is turned off, the air speed is reduced to 20 m/s, and the spin rig is accelerated at 100 RPM/s until accelerometers on the test section walls detect a shed event. The experiments were repeated 6 – 7 times per wire cloth sample. Note that due to COVID-19 related time constraints, the monolithic control sample was only tested twice in the wind tunnel.

The force, F, and shear stress, τ, required to shed ice from a sample are then calculated using Equations (1) and (2):

$$F_{\mathrm{shed}} = \left(\frac{2\pi}{60}\mathrm{RPM}_{\mathrm{shed}}\right)^2 \cdot M_{\mathrm{ice}} \cdot r_{\mathrm{arm}} \tag{1}$$

$$\tau_{\text{shed}} = \frac{F_{\text{shed}}}{A_{\text{ice}}} \tag{2}$$

The mass, M, and contact area, A, of the accumulated ice are determined in preliminary experiments where ice is accreted in the same manner, followed by weighing of the test probe and measuring of its iced interface. The amount of ice accumulated in a given exposure time in the icing cloud has been shown to be very repeatable.

RESULTS AND DISCUSSION

Wire Cloths as Ice-Shedding Surfaces

Woven wire cloth substrates were chosen for this study because the 3-dimensional woven wire matrix imparts two important characteristics: (i) pores are formed throughout the ice—stainless-steel interface; and (ii) the morphology present at the ice—stainless-steel interface is composed of smooth weft wires. It is hypothesized that the combination of these two properties will lead to facile shedding of adhered ice through the induction and advancement of cracks at the ice-cloth interface. As shown in Table 1, differing combinations of warp and weft wire diameters lead to substrates of differing imperial mesh numbers and different warp wire spacings, pore diameters, and number of pores per unit area. However, interestingly our microCT analyses of these three materials show that they possess very similar total surface areas. As such, we can logically compare the ice shedding properties of the cloths through the measured peak dislodging force normalized to the geometric surface area of the ice column (i.e. their ice adhesion strengths).

Table 1. Geometric properties of the woven wire cloths tested in this study

Mesh Number	Warp Diameter [μm]	Weft Diameter [μm]	Warp Spacing [μm]	Equivalent Pore Diameter [μm]	Total Area vs. Geometric [μm/μm]	Number of Pores [pores/mm^2]
200x1400	71	41	145	15	3.71	213
325x2300	36	25	80	9	3.79	513
400x2800	25	20	68	7	3.7	750

As shown in Figure 4 A, the mean ice adhesion strengths measured on the woven wire cloths are indeed significantly lower than those measured on the monolithic, rigid stainless-steel control sample. This is true whether the ice adhesion test was performed using the benchtop thermoelectric rig, or within the altitude icing wind tunnel. The coarsest (i.e. 200x1400) cloth presents with the most dramatic reduction in ice adhesion strengths, where a 95% reduction is measured versus the control. In fact, the 12 ± 3 kPa ice adhesion strength measured on the 200x1400 cloth within the wind tunnel is well below the threshold quoted by some for passive ice removal. These results follow well what has been reported by Ling et al. [14]. Figure S1 presents exemplar force-versus-time graphs for the monolithic control sample and the 200x1400 wire cloth substrates. Superimposed on these graphs are still images of overhead videos we took during the tests which confirm that the low ice adhesion strengths measured are not the result of an induced bending moment in the ice column.

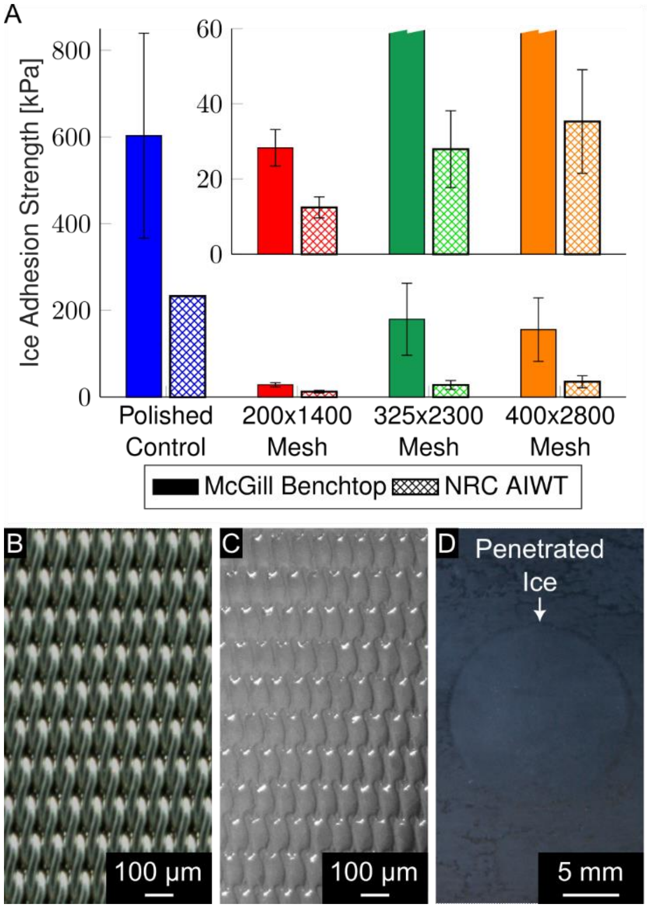

Figure 4. (A) Average measured ice adhesion strength on the woven stainless-steel wire cloths in comparison with a polished control sample. The data is presented for the experiments performed on the benchtop thermoelectric plate and in the altitude icing wind tunnel (AIWT). Error bars represent 95% confidence intervals on the mean. (B) Photograph of the 200x1400 wire cloth immediately after having dislodged an ice column. No remnants of ice are visible on the surface. (C) Photograph of the shed ice interface. Despite some melting, a distinct negative impression of the wire cloth is left behind. (D) Photograph of the thermoelectric plate after removing an iced wire cloth wherein a faint ring imprint shows that water/ice penetrates the 3d microstructural network completely.

Figure 4 B presents a high-magnification photograph of the 200x1400 cloth immediately after having dislodged an ice column on the benchtop setup. This exemplar photo shows that ice cleanly sheds from the wire cloths, with no ice remnants left on the wires. Furthermore, great care was taken to photograph the interface of the ice column in a timely manner after dislodging it from the 200x1400 cloth. As shown in Figure 4 C, despite some melting which occurred before the photo could be captured, a perfect negative impression of the wire cloth interface is left in the ice. Figure 4 B and C together show that it is largely adhesional failure at the ice—stainless-steel wire interface which occurs when the ice is shed.

The ice-shedding properties exhibited by the woven wire cloths is particularly interesting in that their surface areas are substantially higher than the polished, flat control sample. Indeed, an exemplar photograph in Figure 4 D taken of the aluminum plate on which the wire cloths were clamped for the ice adhesion tests reveals that water completely penetrates the 3D-microstructural wire network. This photograph, taken immediately after the ice column is dislodged, shows a perfect circular impression of ice left underneath the column's footprint. We can conclude that there is no air-trapping effect which is leading to the low ice adhesion strengths measured; the ice is in direct contact with the wire cloths' surface area, which is nearly four times the surface area of the polished, monolithic control sample. Thus, without doubt there is ice present within the pores of the wire mesh which had cohesively failed from the bulk ice in the dislodged column. However, we conjecture that this cohesive failure within the pores formed by the woven wires is an integral component of the low-strength ice-shedding process.

Mechanism of Ice-Shedding from Woven Wire Cloths

Our hypothesis has been that the exceptional ice-shedding property of the bare stainless-steel wire cloths stems from the interaction of the forming ice and the morphologies of the 3D-microstructural networks. To this end, we collected microCT data of the wire cloths to exactly visualize the pores formed by the woven wires, and thus the 3-dimensional space occupied by water then ice. Figure 5 A presents a cropped sequence of image slices from the scan of the 200x1400 wire cloth. This sequence shows the morphology of a single pore which is formed between adjacent warp wires and the weft wires woven around them. An animation of this sequence is included as supplementary information. Visualizing the woven wire network in this manner allows us to see that the pores have triangular openings which are bound by three wires: (i) a warp wire, (ii) weft wire 1 woven above one warp wire and below another, and (iii) weft wire 2 running above two warp wires. As we move further into the pore, this triangular cross-section gives way to a larger area underneath weft wire 2 above and the crossing weft wires 2 and 3 below. Further into the sequence, weft wires 2 and 3 have crossed, and a triangular opening is formed at the opposite end. The re-entrant morphology of the woven wire cloths' pores (that is, smaller cross-sections at the openings than in the bulk) is important in the context of water completely infiltrating the network and freezing. The hypothesized process by which ice forms around the wire cloths is presented in Figure 5 B. The woven wire cloths' morphology and the re-entrant nature of their pores create two different areas of ice growth with two different rates: the faces of the cloth and within the network.

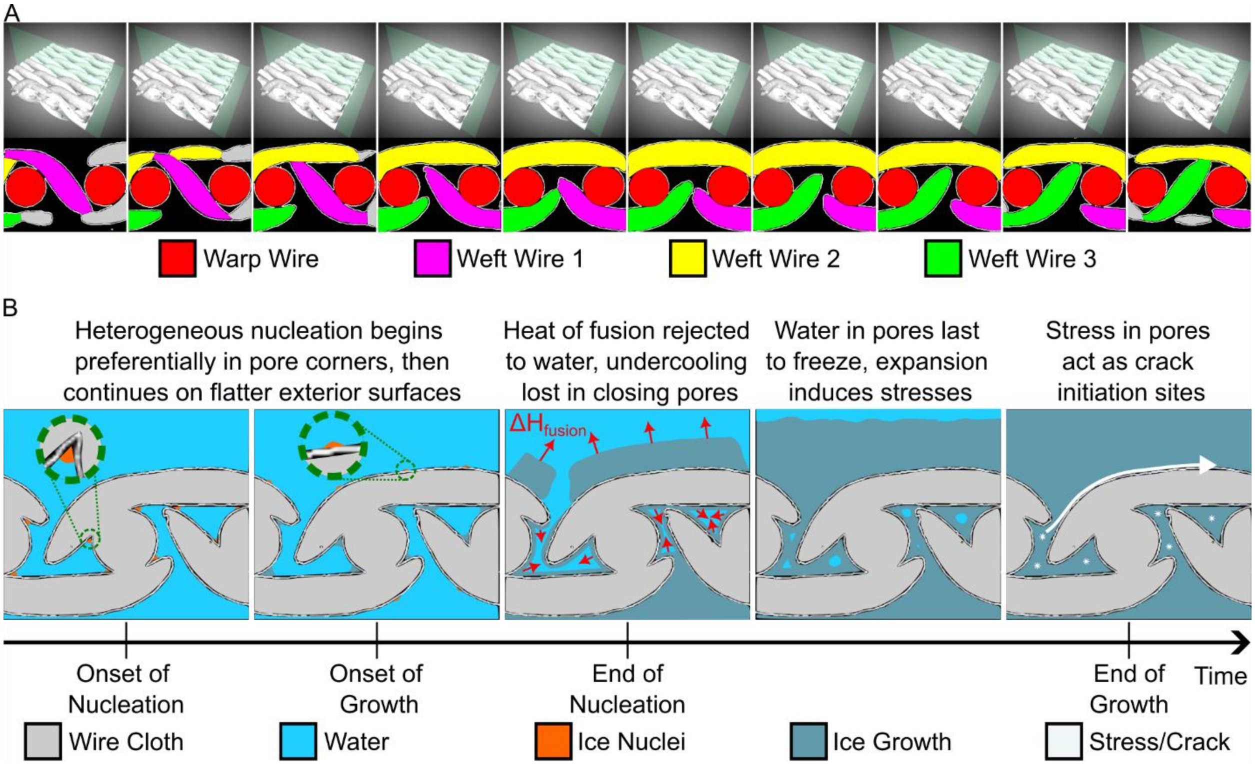

Figure 5. (A) Sequential microCT slices of a pore within the 200x1400 wire cloth showing that the pore openings have a smaller dimension than the cross-sections of the bulk pore – a re-entrant structure. (B) Proposed mechanism for the ice-shedding properties exhibited by the woven wire cloths. Freezing of water within the 3D network of the wire cloths results in stresses in each pore and thus the induction of cracks at the ice—stainless-steel interface.

Ice formation begins with nucleation once some supercooling of the water has occurred below the equilibrium melting temperature and some nucleation time has passed such that a critical embryo radius is achieved [33]. As shown in Figure 5 B, nucleation of this new thermodynamic phase will preferentially occur heterogeneously on the surface of the cold stainless-steel wires. The free energy barrier for the formation of stable nuclei is lowest within the pores where wires meet, and interfacial area is the highest [34-36]. Here the degree of requisite undercooling is the lowest. Nucleation of stable nuclei on the surface of the weft wires making up the face of the wire cloth will occur after further undercooling of the water, when the free energy barrier is sufficiently reduced.

Once a critical size of ice embryo has been reached, it is thermodynamically favourable for their size to increase and thus the growth phase is started. Figure 5 B shows schematically that the continued growth of the ice phase requires continued transfer of the heat of fusion away from the growth front [34]. The latent heat generated is removed more quickly from the ridges formed by the weft wires than in the valleys between [37-39]. As such, even though nucleation will begin in the pores, the rate of growth will be highest from the weft wires on the face of the wire cloth. A cap of ice would be expected to form across the face of the cloth before complete icing of the volume between weft wires or within pores [39]. We expect that the water within the re-entrant pores will be the last to freeze, as the latent heat of fusion generated within them is slowly removed once the pore openings freeze closed.

We hypothesize that it is this final delayed freezing of segregated water within the wire cloth pores that is partly responsible for the low ice adhesion strengths which are manifested. As demonstrated in Figure 5 B, the ice region surrounding the isolated water will be subjected to very large circumferential tensile stresses due to the expansion produced by the progressive freezing of the water [40]. Inclusions formed in the ice within the pores of the woven wire cloths would act as crack nucleation sites [41]. That is, once an external force is applied to the adhered ice, the resulting stress is distributed throughout the material, apart from areas with defects, such as those inclusions formed within the cloth pores. These defective areas act as local stress concentrators, from whence crack nucleation will preferentially occur [7, 14, 42]. A major portion of the induced elastic energy around these defects leads to the opening of the cracks, with the weft wires offering an easy path to follow at the ice-substrate interface. We explicitly note here an important difference between our hypothesized mechanism for the shedding of ice from the woven wire cloth substrates and the mechanisms presented in prior works for the shedding of ice from elastomeric (or elastomer-like metal) substrates. Here, cracks are initiated during the ice formation process, and are then opened once an external force is applied. We see no evidence of macro-scale surface deformation during these steps (Figure S1). In the case of elastomers, the interfacial cracks are induced and opened through a mismatch in stiffness between the adhered ice and substrate, with a higher degree of substrate deformation leading to reduced ice adhesion strengths [24, 25, 27, 31]. Moreover, it is important to note that with the hypothesized introduction of crack nucleation sites at each pore in the wire cloth, each initiated crack needs only propagate the distance to the next warp wire – where the next crack was initiated – to completely de-laminate the adhered ice.

Effect of Surface Material of Construction

We began to test our hypothesis that it is the 3D-microstructural network formed by the woven wires which is imparting the observed ice-shedding properties by fabricating substrates with different metallic surfaces. We used electron beam deposition to coat our materials with 5–10 nm of copper, aluminum, and titanium. In doing so, we were able to create two sets of substrates – derived from either the flat polished stainless-steel coupon, or 200x1400 stainless-steel wire cloth backbone – with consistent surface morphology and crack nucleation sites, while varying the surface chemistry on the top face of the substrates.

Indeed, as shown in Figure 6 the average ice adhesion strength measured on these coated substrates fall into two sets: the polished monolithic coupons, and the porous wire cloths. Based on the thermodynamic work of ice adhesion, one would expect some difference between the ice adhesion strengths exhibited by the different polished metals [43]. Nonetheless, there is no statistically-significant difference in the stress required to shed ice from any of the monolithic coupons – regardless of the metallic surface coating. Similarly, all the 200x1400 cloth substrates present with statistically equivalent ice adhesion strengths, albeit drastically lower than the monolithic samples. These results begin to show that the properties of the surface structure – such as beneficial porosity and morphology – are the key to realizing ice-shedding surfaces.

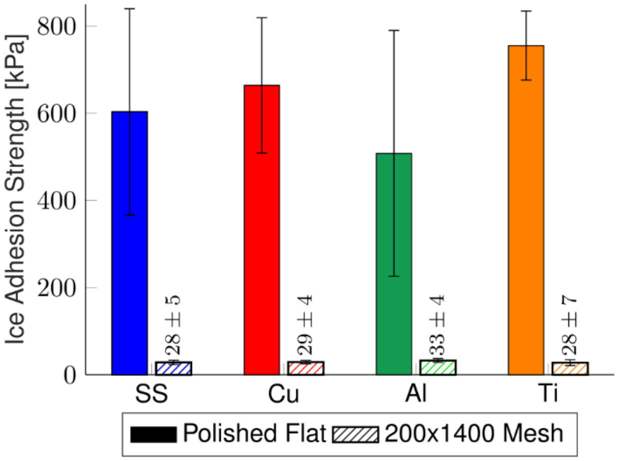

Figure 6. Average ice adhesion strength measured on 200x1400 woven wire cloths and monolithic polished coupons with: stainless-steel, copper, aluminum, and titanium surfaces reveal ice-shedding properties present regardless of metallic surface. Error bars represent 95% confidence intervals on the mean.

The role of crack nucleation and opening in ice shedding

We next sought to isolate the effects of the pores from the topography of the woven wire cloth substrates. The first way in which we isolated these effects was by creating a negative of the

200x1400 wire cloth via PDMS soft lithography from which we molded polypropylene positive replicas (Figure **7** B-C). In doing so, we have fabricated substrates which possess the same gently curving topography of the wire cloths, while eliminating the pores formed at each weaving point of the stainless-steel wires. We added a metallic interface to one of these molded substrates by depositing 5-10 nm of Ti. We measured the average ice adhesion stress on these replica surfaces in comparison with monolithic, polished samples of the same materials and 200x1400 wire cloths of the same metallic interfaces.

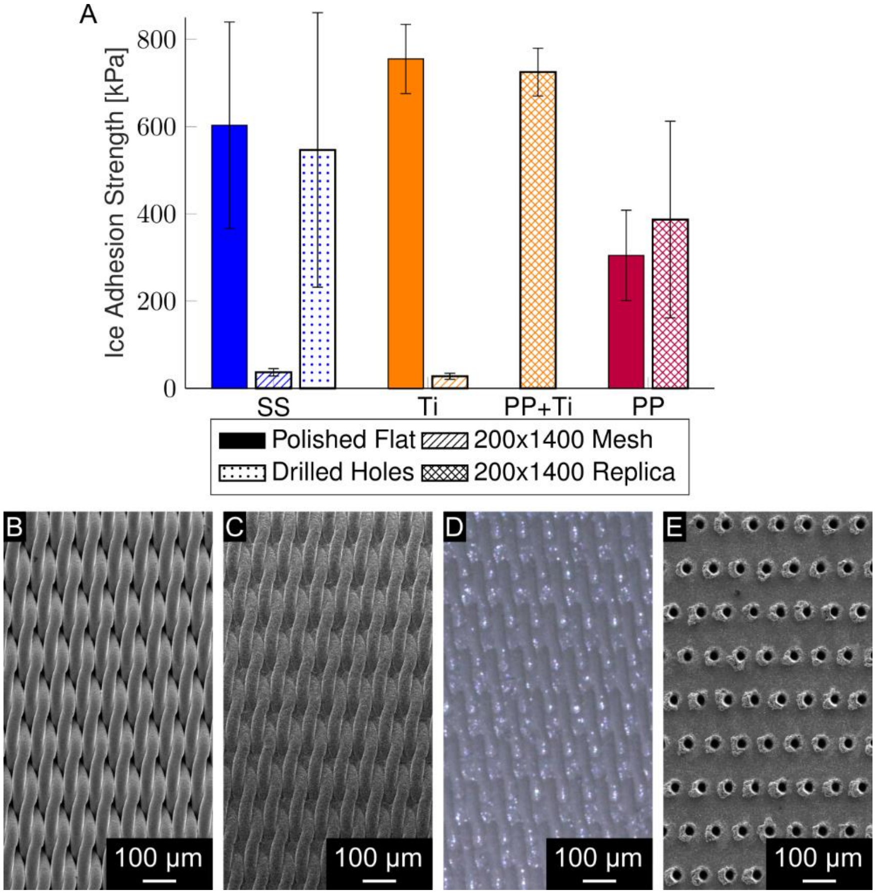

Figure 7. (A) Average ice adhesion strength measured on polypropylene (PP) surfaces which were replica molded from the 200x1400 wire cloth in comparison with smooth samples of the same materials show that ice shedding properties of the wire cloths are lost when the pores are removed. Error bars represent 95% confidence intervals on the mean. (B)-(C) Scanning electron micrographs

of the 200x1400 wire cloth and the replica molded polypropylene substrate. (D) Photograph of ice interface shed from replica molded polymer substrate. Despite lack of crack nucleation sites, topography results in adhesional failure at the ice-substrate interface. (E) Scanning electron micrograph of the laser percussion drilled monolithic sample with through holes in the same layout as the pores of the 200x1400 wire cloth.

Interestingly, as shown in Figure 7 A, elimination of the pores from the titanium-coated substrate has removed with it any ice-shedding characteristics. The replica molded sample coated with titanium (PP+Ti, orange cross-hatch bar) presents with an ice adhesion strength which is statistically equivalent to that measured on the polished monolithic sample coated with titanium (Ti, solid orange bar). We see a similar result on the bare polypropylene replica (PP, pink cross-hatch bar) which analogously presents with equivalent ice adhesion strengths to a polished monolithic polypropylene surface (PP, solid pink bar). These results show the importance of the pores in shedding ice from the woven wire cloths. Without pores, the interfacial cracks are initiated exclusively at the periphery of the bonded area, therefore cracks must open along the entire bonded length for de-lamination to occur.

A final interesting observation was made during testing of the polymer replicas. We noted that, notwithstanding the increased ice adhesion strength versus the stainless-steel wire cloths, ice was indeed cleanly shed from the polymer replicas. An exemplar high-magnification photograph in Figure 7 D of the ice interface immediately after having been dislodged reveals a perfect impression of the replica’s surface topography. That is, the ice-substrate bond has still undergone a majority adhesional failure. This is, perhaps, an important reminder that the opening crack will follow a path of least-resistance [44]. A topography such as the one formed by the gently curving wires of the wire cloths is devoid of sharp corners, where a crack can propagate along the interface without having to deflect to a large degree, avoiding any ice-substrate interlocking effects. The choice of topography, alongside our hypothesis of crack-nucleating pores combine to result in a surface which cleanly sheds ice.

The second way in which we isolated the effects of the pores in ice shedding was by laser percussion drilling holes through a coupon of the polished monolithic stainless-steel material. As shown in Figure 7 E, the holes were micromachined in the same layout as the pores of the 200x1400 wire cloth. Figure S2 provides a micrograph of the backside of this sample which clearly shows that these pores are indeed through holes. As presented in Figure 7 A, this laser micromachined substrate does not shed ice. Figure S3 presents photographs of cobalt chloride test paper laid behind the drilled hole sample during one of the ice adhesion tests. The blue-to-pink colour change of the test paper confirms that water/ice has penetrated the pores machined in the stainless-steel coupon, much like the behaviour on the woven wire cloths. However, this surface is lacking the necessary features to induce interfacial cracks; the surface does not have a morphology which leads to beneficial stress concentration in the pores upon freezing of the infiltrated water. Rather, pores such as these lead to interlocking of the ice with the substrate. In fact, the exemplar photograph of Figure S4 reveals that the ice breaks rather cohesively from the drilled hole coupon, leaving behind many ice remnants on the surface.

Effect of repeated icings

Heretofore the repeated testing of ice shedding from the woven wire cloth materials involved warming the substrates to room temperature, and completely drying them between cycles. As tests, we wanted to see how the woven wire cloths would perform against repeated cycles of icing, without removing any embedded ice. We tested this in two ways. The first, which we call "pre-iced" was to mount the 200x1400 wire cloth onto the benchtop ice adhesion rig, completely flood the substrate with water and allow the system to freeze. We removed any ice on the face of the cloth before proceeding to grow an ice column and measure the ice adhesion strength. Once such an experiment was concluded, we warmed the substrate to room temperature and dried the cloth before proceeding to the next replicate (5 in total). As shown in Figure 8, the surfaces treated in this manner present with statistically equivalent ice adhesion strengths as the standard test.

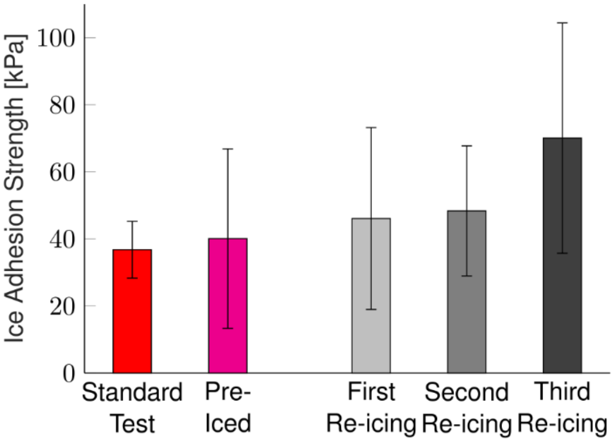

Figure 8. Average ice adhesion strength measured on the 200x1400 wire cloth with embedded ice already present in the microstructural wire network. Error bars represent 95% confidence intervals on the mean. The presence of ice in the pores of the cloth does not lead to increased ice adhesion strengths.

The second way in which we tested the effect of ice already being present in the pores was to immediately proceed with growing a new ice column on the same location of the cloth where the last column was just removed, which we call “re-icing”. We performed the standard test followed by three re-icings (and each of these in five replicates). Like the results for pre-icing, Figure 8 shows that re-icing the surface does not lead to a statistically significant increase in the measured ice adhesion strength. We do note that there does, however, appear to be a slight increasing trend in the mean of the measured data with continued re-icing. A fact that warrants further testing.

We hypothesize that the lack of increased ice adhesion strength in the pre-icing and re-icing results are due to localized melting within the pores with each cycle of the experiment. That is, any ice left embedded in the pores after the dislodging of the bulk ice column is melted and must re-freeze with the water added in the next cycle of the experiment. As such, our hypothesized mechanism for freezing within and around the wire networks restarts and crack nucleating sites are in turn re-formed at each pore. We note that the benchtop rig has a few experimental limitations. The first is that a top cover must be removed to add water to the system/dislodge the ice columns with the force probe. The system is invariably exposed to warm lab air during these steps, and this may be the time when melting can occur within the pores. The second limitation is the manner in which water is added to the system. Supercooled water is picked up by a syringe, mounted into a syringe pump and then added dropwise to the glass mold. The water undoubtedly warms during these steps, and this also may be the time when melting occurs within the pores.

Nonetheless, the pre-icing and re-icing experiments are interesting in that they show that with only minimal energy input, surfaces such as the woven wire cloths can be made to shed ice over multiple cycles. One can envision a semi-active system which only requires localized melting of pores to de-ice a surface rather than large scale heating of an interface.

CONCLUSIONS

In this work we have moved away from the current research paradigms to develop a novel approach to engineering ice-shedding surfaces. Instead of focusing immediately on low surface energy coatings to lower the thermodynamic work of ice adhesion or imparting a high degree of surface roughness to limit ice-substrate contact area, we have viewed the basic problem of ice adhesion through the practical lens of how ice forms, and how this can be manipulated to increase fracturing at the ice-substrate interface. Our work with bare metallic substrates has shown that surfaces which are engineered to promote stress concentrations throughout the iced interface, and therefore nucleate cracks, can lead to extremely low ice adhesion strengths – fulfilling the requirements for passive ice removal. Furthermore, we have shown that this ice-shedding phenomenon is sustained over multiple cycles with only minimal melting required within the pores to re-initialize the crack nucleating process. Starting first with this solidification dynamics approach to ice-shedding surface engineering and only then tuning the surface chemistry, we may see new benchmarks set for low ice adhesion strength surfaces.

Supporting Information

Exemplar force-versus-time graphs for the dislodging of ice from stainless-steel and polypropylene samples. Scanning electron micrograph of the backside of the percussion drilled stainless-steel coupon. Photographs of the cobalt chloride ice penetration tests on the percussion drilled sample. Exemplar photograph of the percussion drilled surface after dislodging ice. (.pdf) Animated walk-throughs of wire cloth micro CT, sliced in XY and YZ planes (.gif).

Author Contributions

M.J.W., P.S., and A.-M.K. conceived the study. M.J.W. designed the experiments. M.J.W. and G.B. performed the experiments. M.J.W. wrote the manuscript. P.S. and A.-M.K. reviewed and edited the manuscript. P.S. and A.-M.K. supervised the study. All authors have given approval to the final version of the manuscript.

Funding Sources

This work was supported by a Natural Sciences and Engineering Research Council of Canada (NSERC) Discovery Grant (RGPIN-2016-04641).

ACKNOWLEDGMENT

We thank C. Moraes and N. Lin (McGill University Cellular Microenvironment Design Laboratory) for their aid in the PDMS soft lithography. We thank C. Clark, D. Orchard, and G. Chevrette (National Research Council Canada Aerospace Research Center) for their aid in the Altitude Icing Wind Tunnel tests.

REFERENCES

1. Wood, M.J.; A.-M. Kietzig. Factors Influencing the Formation, Adhesion, and Friction of Ice. In *Ice Adhesion: Mechanisms, Measurement and Mitigation*.; Wiley, 2020; pp 1-54.
2. Thomas, S.K.; R.P. Cassoni; C.D. MacArthur. Aircraft Anti-Icing and De-Icing Techniques and Modeling. J. Aircr. **1996**, 33 (5), 841-854. DOI: 10.2514/3.47027
3. Hejazi, V.; K. Sobolev; M. Nosonovsky; From Superhydrophobicity to Icephobicity: Forces and Interaction Analysis. Sci. Rep. **2013**, 3 (1), 2194. DOI: 10.1038/srep02194
4. Sojoudi, H.; Wang, M.; Boscher, N.D.; McKinley, G.H.; Gleason, K.K.; Durable and Scalable Icephobic Surfaces: Similarities and Distinctions from Superhydrophobic Surfaces. Soft Matter **2016**, 12 (7), 1938-1963. DOI: 10.1039/c5sm02295a
5. Dou, R.; Chen, J.; Zhang, Y.; Wang, X.; Cui, D.; Song, Y.; Jiang, L.; Wang, J.; Anti-Icing Coating with an Aqueous Lubricating Layer. Appl. Mater. Interfaces **2014**, 6 (10), 6998-7003. DOI: 10.1021/am501252u
6. Boluk, Y.; *Adhesion of Freezing Precipitates to Aircraft Surfaces*; Canadian Air Transportation Administration Civil Aviation Branch, Transportation Development Centre: Montréal, QC, 1996.
7. Menini, R.; Farzaneh, M.; Advanced Icephobic Coatings. J. Adh. Sci. Technol. **2011,** 25 (9), 971-992. DOI: 10.1163/016942410X533372
8. Zhu, L.; Xue, J.; Wang, Y.; Chen, Q.; Ding, J.; Wang, Q.; Ice-phobic Coatings Based on Silicon-Oil-Infused Polydimethylsiloxane. Appl. Mater. Interfaces **2013**. 5 (10), 4053-4062. DOI: 10.1021/am400704z
9. Wong, T.-S.; Kang, S.H.; Tang, S.K.Y.; Smythe, E.J.; Hatton, B.D.; Grinthal, A.; Aizenberg, J.; Bioinspired Self-Repairing Slippery Surfaces with Pressure-Stable Omniphobicity. Nature **2011**, 477 (7365), 443-447. DOI: 10.1038/nature10447
10. Bharathidasan, T.; Kumar, S.V.; Bobji, M.S.; Chakradhar, R.P.S.; Basu, B.J.; Effect of Wettability and Surface Roughness on Ice-Adhesion Strength of Hydrophilic, Hydrophobic and Superhydrophobic Surfaces. Appl. Surf. Sci. **2014**, 314, 241-250. DOI: 10.1016/j.apsusc.2014.06.101
11. Kim, P.; Wong, T.-S.; Alvarenga, J.; Kreder, M.J., Adorno-Martinez, W.E.; Aizenberg, J.; Liquid-Infused Nanostructured Surfaces with Extreme Anti-Ice and Anti-Frost Performance. ACS Nano **2012**, 6 (8), 6569-6577. DOI: 10.1021/nn302310q
12. Coady, M.J.; Wood, M.J.; Wallace, G.Q.; Nielsen, K.E.; Kietzig, A.-M.; Lagugné-Labarthet, F.; Ragogna, P.J.; Icephobic Behavior of UV-Cured Polymer Networks Incorporated into Slippery Lubricant-Infused Porous Surfaces: Improving SLIPS Durability. Appl. Mater. Interfaces **2018**, 10 (3), 2890-2896. DOI: 10.1021/acsami.7b14433
13. Kreder, M.J.; Alvarenga, J.; Kim, P. Aizenberg, J.; Design of Anti-Icing Surfaces: Smooth, Textured or Slippery? Nat. Rev. Mater. **2016,** 1 (1), 15003. DOI: 10.1038/natrevmats.2015.3
14. Ling, E.J.Y.; Uong, V.; Renault-Crispo, J.-S.; Kietzig, A.-M.; Servio, P.; Reducing Ice Adhesion on Nonsmooth Metallic Surfaces: Wettability and Topography Effects. Appl. Mater. Interfaces **2016,** 8 (13), 8789-8800. DOI: 10.1021/acsami.6b00187
15. Farhadi, S.; Farzaneh, M.; Simard, S.; On Stability and Ice-Releasing Performance of Nanostructured Fluoro-Alkylsilane-Based Superhydrophobic Al Alloy2024 Surfaces. IJTAN **2012,** 1 (1), 38-44. DOI: 10.11159/ijtan.2012.006

16. Davis, A.; Yeong, Y.H.; Steele, A.; Bayer, I.S.; Loth, E.; Superhydrophobic Nanocomposite Surface Topography and Ice Adhesion. Appl. Mater. Interfaces **2014,** 6 (12), 9272-9279. DOI: 10.1021/am501640h
17. Wang, Y.; Xue, J.; Wang, Q.; Chen, Q.; Ding, J.; Verification of Icephobic/Anti-icing Properties of a Superhydrophobic Surface. Appl. Mater. Interfaces **2013,** 5 (8), 3370-3381. DOI: 10.1021/am400429q
18. Susoff, M.; Siegmann, K.; Pfaffenroth, C.; Hirayama, M.; Evaluation of Icephobic Coatings—Screening of Different Coatings and Influence of Roughness. Appl. Surf. Sci. **2013,** 282, 870-879. DOI: 10.1016/j.apsusc.2013.06.073
19. Kulinich, S.A.; Farhadi, S.; Nose, K.; Du, X.W.; Superhydrophobic Surfaces: Are They Really Ice-Repellent? Langmuir **2011,** 27 (1), 25-29. DOI: 10.1021/la104277q
20. Pruppacher, H.R.; Klett, J.D.; Microstructure of Atmospheric Clouds and Precipitation. In *Microphysics of Clouds and Precipitation*.; Springer, 2010; pp. 10-73.
21. Wang, H.-J.; Xi, X.K.; Kleinhammes, A.; Wu, Y.; Temperature-Induced Hydrophobic-Hydrophilic Transition Observed by Water Adsorption. Science **2008,** 322 (5898), 80-83. DOI: 10.1126/science.116241
22. Golovin, K.; Dhyani, A.; Thouless, M.D.; Tuteja, A.; Low–Interfacial Toughness Materials for Effective Large-Scale Deicing. Science **2019**, 364 (6438), 371-375. DOI: 10.1126/science.aav1266
23. Mohseni, M.; Recla, L.; Mora, J.; Gallego, P.G.; Agüero, A.; Golovin, K.; Quasicrystalline Coatings Exhibit Durable Low Interfacial Toughness with Ice. Appl. Mater. Interfaces **2021**, 13 (30), 36517-36526. DOI: 10.1021/acsami.1c08740
24. Golovin, K.; Kobaku, S.P.R.; Lee, D.H.; Diloreto, E.T.; Mabry, J.M.; Tuteja, A.; Designing Durable Icephobic Surfaces. Sci. Adv. **2016**, 2 (3), e1501496. DOI: 10.1126/sciadv.150149
25. Irajizad, P.; Al-Bayati, A.; Eslami, B.; Shafquat, T.; Nazari, M.; Jafari, P.; Kashyap, V.; Masoudi, A.; Araya, D.; Ghasemi, H.; Stress-Localized Durable Icephobic Surfaces. Mater. Horiz. **2019**, 6 (4), 758-766. DOI: 10.1039/c8mh01291a
26. Sivakumar, G.; Jackson, J.; Ceylan, H.; Sundararajan, S.; An Investigation on Ice Adhesion and Wear of Surfaces with Differential Stiffness. Wear **2021**, 476, 203662. DOI: 10.1016/j.wear.2021.203662
27. He, Z.; Xiao, S.; Gao, H.; He, J.; Zhang, Z.; Multiscale Crack Initiator Promoted Super-Low Ice Adhesion Surfaces. Soft Matter **2017,** 13 (37), 6562-6568. DOI: 10.1039/C7SM01511A
28. He, Z.; Zhuo, Y.; He, J.; Zhang, Z.; Design and Preparation of Sandwich-Like Polydimethylsiloxane (PDMS) Sponges with Super-Low Ice Adhesion. Soft Matter **2018**, 14 (23), 4846-4851. DOI: 10.1039/c8sm00820e
29. He, Z.; Zhuo, Y.; Wang, F.; He, J.; Zhang, Z.; Understanding the Role of Hollow Sub-Surface Structures in Reducing Ice Adhesion Strength. Soft Matter **2019**, 15 (13), 2905-2910. DOI: 10.1039/C9SM00024K
30. He, Z.; Zhuo, Y.; Wang, F.; He, J.; Zhang, Z. Design and Preparation of Icephobic PDMS-Based Coatings by Introducing an Aqueous Lubricating Layer and Macro-Crack Initiators at the Ice-Substrate Interface. Prog. Org. Coat. **2020**, 147, 105737. DOI: 10.1016/j.porgcoat.2020.105737

31. Zarasvand, K.A.; Pope, C.; Mohseni, M.; Orchard, D.; Clark, C.; Golovin, K.; Metallic Plate Buckling As a Low Adhesion Mechanism for Durable and Scalable Icephobic Surface Design. Adv. Mater. Interfaces **2022**, 9 (1), 2101402. DOI: 10.1002/admi.202101402
32. Zalouk, M.; Ice Adhesion on Amphiphilic Methacrylate Copolymer Surfaces. Masters Thesis, McGill University, Montréal, QC, 2019. https://escholarship.mcgill.ca/concern/theses/rx913s15k (accessed 2022-07-72).
33. Karthika, S.; Radhakrishnan, T.K.; Kalaichelvi, P.; A Review of Classical and Nonclassical Nucleation Theories. Cryst. Growth Des. **2016**, 16 (11), 6663-6681. DOI: 10.1021/acs.cgd.6b00794
34. Glicksman, M.E.; Dendritic Growth. In *Handbook of Crystal Growth,* 2nd ed.; Elsevier, 2015; pp. 669-722.
35. Tavakoli, F.; Davis, S.H.; Kavehpour, H.P.; Freezing of Supercooled Water Drops on Cold Solid Substrates: Initiation and Mechanism. JCTR **2015**, 12 (5), 869-875. DOI: 10.1007/s11998-015-9693-0
36. Mullin, J.W.; Nucleation. In *Crystallization,*4th ed.; Butterworth-Heinemann, 2001; pp. 181-215.
37. Maddox, J.; Snowflakes Are Far From Simple. Nature **1983**, 306 (5938), 13-13. DOI: 10.1038/306013a0
38. Mullins, W.W.; Sekerka, R.F.; Stability of a Planar Interface During Solidification of a Dilute Binary Alloy. In *Dynamics of Curved Fronts*.; Academic Press, 1988; pp. 345-352.
39. Wong, W.S.Y.; Hauer, L.; Cziko, P.A.; Meister, K.; Cryofouling Avoidance in the Antarctic *Scallop Adamussium colbecki.* Natur. Commun. Biol. **2022**, 5 (1), 83. DOI: 10.1038/s42003-022-03023-6
40. Picu, R.C.; Gupta, V.; Frost, H.J.; Crack Nucleation Mechanism in Saline Ice. J. Geophys. Res. Solid Earth **1994**, 99 (B6), 11775-11786. DOI: 10.1029/94JB00685
41. Frost, H.J.; Mechanisms of Crack Nucleation in Ice. Eng. Fract. Mech. **2001**, 68 (17), 1823-1837. DOI: 10.1016/S0013-7944(01)00036-4
42. Nosonovsky, M; Hejazi, V.; Why Superhydrophobic Surfaces Are Not Always Icephobic. ACS Nano **2012**, 6 (10), 8488-8491. 10.1021/nn302138r
43. Makkonen, L.; Ice Adhesion —Theory, Measurements and Countermeasures. J. Adhes. Sci. Technol. **2012**, 26 (4-5), 413-445. DOI: 10.1163/016942411X574583
44. Anderson, T.L.; *Fracture Mechanics: Fundamentals and Applications*. 3rd ed; Taylor & Francis, 2005.

Graphical TOC